



LIGHT-SCATTERING FLUCTUATIONS AND NOISE IN NONLINEAR OPTICAL PROCESSING

AD-A279 748**Robert L. McGraw**

**Rockwell International Science Center
1049 Camino Dos Rios
Thousand Oaks, CA 91360**

March 1994

**DTIC
ELECTE
MAY 27 1994**

S G D

Final Report

398 **94-15951**

APPROVED FOR PUBLIC RELEASE; DISTRIBUTION IS UNLIMITED.



**PHILLIPS LABORATORY
LASERS AND IMAGING DIRECTORATE
AIR FORCE MATERIEL COMMAND
KIRTLAND AIR FORCE BASE, NM 87117-5776**

94 5 26 159

DTIC QUALITY INSPECTED 1

This final report was prepared by Rockwell International Science Center, Thousand Oaks, California, under contract F29601-89-C-0085, Job Order 33261B22 with the Phillips Laboratory, Kirtland Air Force Base, New Mexico. The Laboratory Project Officer-in-Charge was Christopher M. Clayton (LITN).

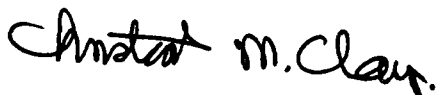
When Government drawings, specifications, or other data are used for any purpose other than in connection with a definitely Government-related procurement, the United States Government incurs no responsibility or any obligation whatsoever. The fact that the Government may have formulated or in any way supplied the said drawings, specifications, or other data, is not to be regarded by implication, or otherwise in any manner construed, as licensing the holder, or any other person or corporation; or as conveying any rights or permission to manufacture, use, or sell any patented invention that may in any way be related thereto.

This report has been authored by a contractor of the United States Government. Accordingly, the United States Government retains a nonexclusive, royalty-free license to publish or reproduce the material contained herein, or allow others to do so, for the United States Government purposes.

This report has been reviewed by the Public Affairs Office and is releasable to the National Technical Information Service (NTIS). At NTIS, it will be available to the general public, including foreign nationals.

If your address has changed, if you wish to be removed from the mailing list, or if your organization no longer employs the addressee, please notify PL/LITN, Kirtland AFB, NM 87117-5776 to help maintain a current mailing list.

This technical report has been reviewed and is approved for publication.

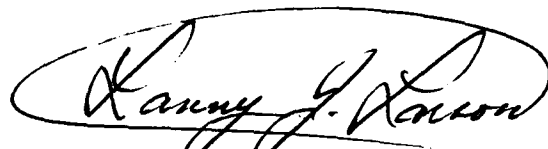


CHRISTOPHER M. CLAYTON
Project Officer

FOR THE COMMANDER



CHRISTOPHER J. COULS, Major, USAF
Chief, Laser Systems Division



LANNY LARSON, Colonel, USAF
Director, Lasers and Imaging
Directorate

DO NOT RETURN COPIES OF THIS REPORT UNLESS CONTRACTUAL OBLIGATIONS OR NOTICE ON A SPECIFIC DOCUMENT REQUIRES THAT IT BE RETURNED.

REPORT DOCUMENTATION PAGEForm Approved
OMB No. 0704-0188

Public reporting burden for this collection of information is estimated to average 1 hour per response, including the time for reviewing instructions, searching existing data sources, gathering and maintaining the data needed, and completing and reviewing the collection of information. Send comments regarding this burden estimate or any other aspect of this collection of information, including suggestions for reducing this burden, to Washington Headquarters Services, Directorate for Information Operations and Reports, 1215 Jefferson Davis Highway, Suite 1204, Arlington, VA 22202-4302, and to the Office of Management and Budget, Paperwork Reduction Project (0704-0188), Washington, DC 20503.

1. AGENCY USE ONLY (Leave blank)		2. REPORT DATE March 1994	3. REPORT TYPE AND DATES COVERED Final Nov 89 - Nov 92	
4. TITLE AND SUBTITLE LIGHT-SCATTERING FLUCTUATIONS AND NOISE IN NONLINEAR OPTICAL PROCESSING			5. FUNDING NUMBERS C: F29601-89-C-0085 PE: 62601F PR: 3326 TA: 1B WU: 22	
6. AUTHOR(S) Robert L. McGraw				
7. PERFORMING ORGANIZATION NAME(S) AND ADDRESS(ES) Rockwell International Science Center 1049 Camino Dos Rios Thousand Oaks, CA 91360			8. PERFORMING ORGANIZATION REPORT NUMBER SC71022.FR	
9. SPONSORING/MONITORING AGENCY NAME(S) AND ADDRESS(ES) Phillips Laboratory 3550 Aberdeen Avenue SE Kirtland AFB, NM 87117-5776			10. SPONSORING/MONITORING AGENCY REPORT NUMBER PL-TR--93-1039	
11. SUPPLEMENTARY NOTES				
12a. DISTRIBUTION/AVAILABILITY STATEMENT Approved for public release; distribution is unlimited.			12b. DISTRIBUTION CODE	
13. ABSTRACT (Maximum 200 words) <p>This report summarizes the results of a 3-yr investigation into the role of light-scattering noise in nonlinear optical processes. These results span a full range -- from physical and mathematical description and prediction of noise properties to experimental verification of the theory and interpretation of measurements. Light-scattering noise fluctuations are shown to set fundamental limits on device size and sensitivity and on beam power requirements for nonlinear optical processes.</p>				
14. SUBJECT TERMS Nonlinear Optics, Noise, Light Scattering, Fluctuations			15. NUMBER OF PAGES 40	
			16. PRICE CODE	
17. SECURITY CLASSIFICATION OF REPORT Unclassified	18. SECURITY CLASSIFICATION OF THIS PAGE Unclassified	19. SECURITY CLASSIFICATION OF ABSTRACT Unclassified	20. LIMITATION OF ABSTRACT	

CONTENTS

Section	Page
1.0 EXECUTIVE SUMMARY	1
2.0 INTRODUCTION	3
3.0 LIGHT-SCATTERING NOISE IN PHOTOREFRACTIVE MEDIA	5
3.1 ORIGINS OF THE PHOTOREFRACTIVE EFFECT	5
3.2 THERMAL FLUCTUATIONS IN THE SPACE-CHARGE FIELD.....	7
3.3 LIGHT-SCATTERING FLUCTUATIONS ASSOCIATED WITH THE PHOTOREFRACTIVE EFFECT.....	7
3.4 LIGHT-SCATTERING FLUCTUATIONS IN PHOTOREFRACTIVE MEDIA ASSOCIATED WITH THE OPTICAL KERR EFFECT	8
3.5 ESTIMATES OF DYNAMIC RANGE AND COMPARISON WITH EXPERIMENT.....	8
4.0 GENERAL THEORY OF LIGHT-SCATTERING NOISE IN KERR MEDIA	14
4.1 LIGHT-SCATTERING FLUCTUATIONS AND NONLINEAR OPTICAL RESPONSE.....	14
4.2 APPLICATION OF THE FLUCTUATION-DISSIPATION THEOREM....	15
5.0 APPLICATIONS TO TWO-WAVE MIXING AND COMPARISON WITH EXPERIMENT.....	18
5.1 THEORY.....	18
5.2 EXPERIMENTAL RESULTS	21
6.0 RESEARCH DIRECTIONS.....	29
REFERENCES.....	33

Accession For	
NTIS	<input checked="" type="checkbox"/>
CRA&I	<input checked="" type="checkbox"/>
DTIC	<input type="checkbox"/>
TAB	<input type="checkbox"/>
Unannounced	<input type="checkbox"/>
Justification	
By	
Distribution /	
Availability Codes	
Dist	Avail and / or Special
A-1	

FIGURES

Figure		Page
1	Light-scattering noise.....	4
2	Photorefractive glasses: comparison of hopping and Kukhtarev models	6
3	Measurements of dynamic range (from Ref. 11).....	9
4	Light-scattering noise simulation (from Ref. 10)	10
5	Two-wave mixing geometry.....	19
6	Schematic diagram of the two-wave mixing optical arrangement and electronics for noise analysis. (L: focusing lens; M1: 100% mirror, PZT: piezo-electric transducer; D: photodiode.).....	22
7	Comparison of experimental and simulation results for two-wave mixing gain and light-scattering noise.....	24
8	The RMS noise power as a function of probe power for $\Omega\tau = 0$. (The experimental data points [triangles] follow a square-root dependence on the probe power [solid curve]. The single data point on the ordinate gives the RMS noise power measured in the absence of the probe beam.)	27
9	Results for damped oscillator, low damping	30
10	Results for damped oscillator, intermediate damping.....	31
11	Results for damped oscillator, high damping.....	32

1.0 EXECUTIVE SUMMARY

This report summarizes the results of a 3-yr investigation into the role of light-scattering noise in nonlinear optical processes. These results span a full range—from physical and mathematical description and prediction of noise properties to experimental verification of the theory and interpretation of measurements. Light-scattering noise fluctuations are shown to set fundamental limits on device size and sensitivity and on beam power requirements for nonlinear optical processes. Fundamental limits to optical phase conjugation and to weak signal amplification via two-wave mixing are derived through a statistical thermodynamic treatment based on the fluctuation-dissipation theorem. In particular, power dissipation in a nonlinear optical medium during the coherent transfer of energy from a pump to a signal beam will be examined, and quantitatively relate this dissipation to the spectrum of quantum/thermal fluctuations that give rise to light-scattering noise. Several classes of nonlinear optical materials are discussed, including resonant and nonresonant Kerr media and photorefractive glasses. Results from experiments carried out at the Science Center and in collaboration with the University of Rome (Rome, Italy) are analyzed and compared with computer simulations of beam propagation and light-scattering noise using the stochastic noise model.

The scientific output from the noise investigations includes two invited presentations (Snowbird and SPIE), numerous contributed papers, and many publications that have appeared in journals such as *Physical Review* (four papers), *Applied Physics Letters* (two papers) and *JOSA B* (two papers). Several additional papers are in the final stages of preparation. The project has been extremely productive both from our own viewpoint and from the many independent reviewers who have assessed the importance of our work, as well as from experimentalists who have undertaken extensive measurements to confirm and extend our results. The experiments of Sternklar et al. (Ref. 1), in particular, present a new application of our results to Brillouin two-beam coupling and confirm our prediction of strong signal-to-noise ratio dependence on pump intensity. Earlier studies of Brillouin amplifiers (e.g., Bespalov et al.) neglected pump dependence. The experiments of Sternklar et al. confirm our fluctuation-dissipation relation for the amplitude of dielectric fluctuations in terms of the temperature, beam interaction volume, and Kerr coefficient (Refs. 2-8). More detailed confirmation can be found in the experiments of Pizzoferrato et al. (Ref. 9), which also examine the frequency dependence of the noise accompanying two-wave mixing in a Kerr medium. The experiments of Chang et al. (Ref. 11) extend the measurements of noise to photorefractive media and confirm the predictions obtained for this class of materials under the present contract.

It is believed that with further development the results will serve as the scientific basis necessary for the design of new low-noise nonlinear optical materials—probably with best prospects in the general classes of photorefractive polymers and charge transfer media. Furthermore, our results can provide the foundation for future investigations into the noise properties of optical communication channels and optical storage media. These future investigations can include determination of the Shannon channel capacity (some work along these lines has already been carried out for photorefractive media) and new applications of optical signal processing and computing (e.g., the optical wavelet transform and optical methods for signal and image compression).

2.0 INTRODUCTION

Most treatments of optical phase conjugation and two-wave mixing do not address the role of noise; others include quantum noise in the incoming electromagnetic fields, but neglect temperature-dependent noise arising from fluctuations inherent in the nonlinear medium itself. Such fluctuations are important to consider to the extent that they reduce the fidelity of an optical signal by giving rise to scattered light.

Studies were done on light-scattering noise for continuous wave (cw) nonlinear optical processes using Kerr and artificial Kerr media (Refs. 2-9) and for similar processes using the photorefractive effect (Refs. 10 and 11). In the former case, a fundamental connection between light scattering fluctuations $\delta\epsilon$ in the medium and the nonlinear dielectric constant ϵ_2 was derived in the form of a static susceptibility relation (Ref. 4) and was applied to a study of light-scattering noise in the phase conjugate signal obtained through degenerate four-wave mixing (Refs. 5 and 6). Time-averaged noise powers were determined and were of order kTv where k is the Boltzmann constant, T is temperature, and v is the optical frequency. At room temperature and visible wavelengths, kTv is in the microwatt range. The static susceptibility between ϵ_2 and $\delta\epsilon$ was extended in a more recent article and applied to four-wave mixing in Kerr media with nonlocal interactions near a critical point (Ref. 5). Throughout the following, the noise arising from the fluctuations $\delta\epsilon$ equivalently will be referred to as either thermal or light-scattering noise.

For many optical signal processing applications a more complete description of noise than is furnished by the time-averaged noise power is desired. This additional information might include, for example, the effect of light-scattering noise fluctuations on the output light intensity of a nonlinear optical device in real time. For image processing applications, such as the use of optical phase conjugation to correct aberration, the effects of light-scattering noise on the amplitude and phase of the electromagnetic field itself must be included. In the following sections, stochastic simulations for light-scattering noise are developed; the simulations provide a direct means through which this additional information may be obtained. In the following sections, the theory of light-scattering noise in Kerr media is extended using the fluctuation-dissipation theorem (Ref. 6). This generalization of the static susceptibility relation is required for applications to time-dependent processes and nonlinear optical media exhibiting power dissipation. An important example of such a process is the amplification of a weak optical signal via the coherent transfer of energy from a strong pump beam during nondegenerate two-wave mixing (Refs. 7-9). Reference 6 presents the basis for stochastic noise simulation using Langevin

and generalized Langevin models to relate the time decay of laser-induced gratings to the thermal fluctuations responsible for light-scattering noise. Applications to the nonlinear optical processes of phase conjugation, via degenerate four-wave mixing (Ref. 6), and to weak signal amplification, via nondegenerate two-wave mixing (Refs. 7-9), were obtained as part of the study.

Figure 1 shows a schematic depiction of the origins of light-scattering noise. The solid arrows show incoming and outgoing signal beams with a volume element of the nonlinear medium while the dashed arrows show the scattered light noise. The amplitudes and time-correlation properties of the signal and noise gratings (fluctuations in the dielectric constant of the medium) are connected through the fluctuation-dissipation relation described below. For Kerr media, the signal response and noise properties are connected via the fluctuation-dissipation theorem to thermal fluctuations in density. For photorefractive media, the signal is connected to thermal fluctuations in the space-charge field. Photorefractive noise, however, is due to scattered light from both thermal fluctuations in the space-charge field and thermal fluctuations in density. Thus for a photorefractive medium, the Kerr coefficient needs to be determined to completely describe the noise (Refs. 10 and 11).

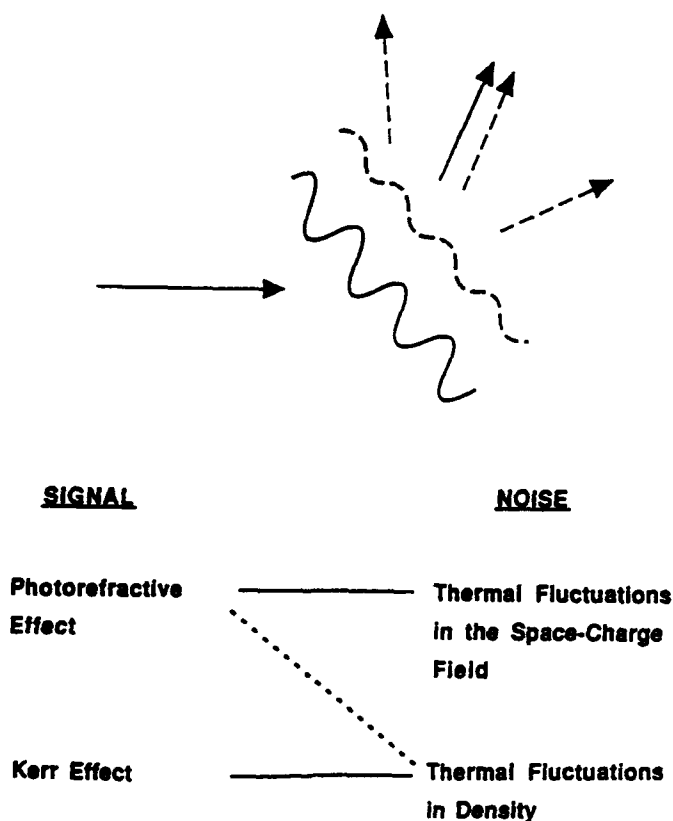


Figure 1. Light-scattering noise.

3.0 LIGHT-SCATTERING NOISE IN PHOTOREFRACTIVE MEDIA

Photorefractive media constitute a large and versatile class of nonlinear optical materials with applications to holographic storage as well as to real-time optical information processing. Two closely related theoretical models of the photorefractive effect have been put forth (Refs. 12 and 13) and successfully used over the past decade by a number of investigators for the description of nonlinear optical processes including optical phase conjugation and coherent beam combination via two-wave mixing. Nevertheless, few studies have been directed at quantifying the fundamental limits to the photorefractive effect set by noise. In particular, questions related to the noise limits on photorefractive sensitivity to weak incident signal powers (dynamic range) apparently have not been addressed. The present study shows that noise limits to the dynamic range of a photorefractive medium are inherent in the photorefractive effect itself. The quantitative determination of these limits is the foremost objective of this section.

3.1 ORIGINS OF THE PHOTOREFRACTIVE EFFECT

Initiation of the photorefractive effect occurs when a spatial variation of light intensity incident on the medium causes a redistribution of charge density and buildup of a space-charge field. For example, let the spatial light intensity distribution follow the simple sinusoidal grating form

$$I(x) = I_0[1 + m \cos(qx)] \quad (1)$$

characterized by average intensity I_0 , grating wave vector q , and intensity modulation ratio m . The intensity grating induces a corresponding density of the form

$$n(x) = n_0[1 + w \cos(qx)] \quad (2)$$

where n_0 is the average density. In the hopping model, n refers to the number density of hopping carriers of charge q_e . In the Kukhtarev model, n refers to the number density of unionized donor sites.

A comparison of the Kukhtarev and hopping models is presented in Figure 2. Each model assumes a uniform population of fixed sites as well as a uniform distribution of fixed countercharges to maintain overall charge neutrality. In the hopping model, the fixed sites may be occupied by a smaller number of mobile carriers of charge q_e . The latter are assumed to hop from site to site with a hopping rate that is proportional to the local light intensity. The net effect is to cause the carriers to diffuse from regions of higher to regions of lower light intensity. As a result, the density modulation ratio w in Equation 2 is opposite in sign to the intensity

modulation ratio, m . In the Kukhtarev model, the fixed sites are occupied with a smaller number of valence band carriers whose charge may be either positive or negative. For definiteness, the carriers in both models are assumed to be electrons of charge $q_e = e = -1e$. Mobility of carriers in the Kukhtarev model requires excitation from the valence band into the conduction band (depicted by the shaded region in Fig. 2) at a rate that is proportional to the light intensity. Generation and recombination of carriers is a fast process compared to the overall redistribution of charge, and the number of carriers in the conduction band at any given time is negligible compared to the number of valence band carriers (donors). Redistribution of charge in the Kukhtarev model may, therefore, be thought of as due to the redistribution of the donor population through accumulated generation, recombination, and transport of carriers via the conduction band. The index change induced by the space-charge field occurs through the Pockels effect as described below.

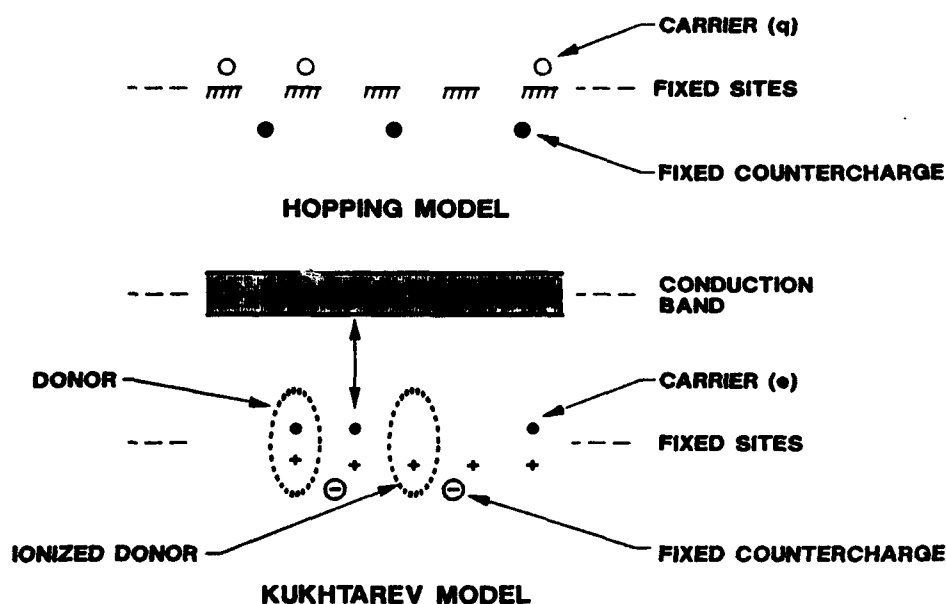


Figure 2. Photorefractive glasses: comparison of hopping and Kukhtarev models.

To simplify the present analysis, contributions to grating formation from the photocurrent, dark current, and externally applied electric fields will be neglected. The contributions from higher order gratings will also be neglected since the primary interest is in the small modulation ratio limit. The various components of the grating free-energy will now be derived. These include contributions from energy storage in the space-charge field, configurational entropy, and the free energy associated with exposure of the donor or hopping sites, depending on which model is used, to a spatially varying light intensity.

3.2 THERMAL FLUCTUATIONS IN THE SPACE-CHARGE FIELD

Fluctuations in the space-charge field are determined by the free-energy change that accompanies the fluctuation. The free energy is, in turn, made up of energy and entropy contributions as described in Reference 10. In the diffusion limit, the energy contribution dominates and thermal fluctuations in the space-charge field may be obtained immediately from the equipartition of energy stored in the space-charge field

$$U_{sc} = (\epsilon_0/8\pi) \int E_{sc}^2(x) dx = (\epsilon_0 V_s/8\pi) \langle |\delta E_{sc}|^2 \rangle = kT/2 \quad (3)$$

In the absence of an entropic contribution, U_{sc} is equal to the free energy. Rewriting the last equality gives

$$\langle |\delta E_{sc}(q)|^2 \rangle_{\text{diff limit}} = (4\pi kT/\epsilon_0 V_s) \quad (4)$$

The general result is (Ref. 10)

$$\langle |\delta E_{sc}(q)|^2 \rangle = (4\pi kT/\epsilon_0 V_s) [1 + (q/k_D)^2]^{-1} \quad (5)$$

where q is the magnitude of the grating wave vector and k_D is the reciprocal Debye length. The difference between Equations 4 and 5 is due to the entropic contribution with the square bracket factor accounting for nonlocal interaction (Ref. 10).

3.3 LIGHT-SCATTERING FLUCTUATIONS ASSOCIATED WITH THE PHOTOREFRACTIVE EFFECT

Dielectric fluctuations that originate from fluctuations in the space-charge field follow immediately from Equation 5 through the Pockels effect

$$\delta\epsilon = \epsilon^{(2)} \delta E_{sc} \quad (6)$$

where $\epsilon^{(2)}$ is related to the electro-optic tensor, r , and the refractive index of the medium, n_R . The standard relations $\Delta n = -(1/2)n_R^3 r E$, for the index change, and $\Delta\epsilon = 2n_R \Delta n$ yield

$$\epsilon^{(2)} = -n_R^4 r \quad (7)$$

Combining Equation 5 for the mean-square fluctuations in the space-charge field with Equation 6 gives

$$\langle |\delta\epsilon(q)|^2 \rangle_{PR} = (4\pi kT/\epsilon_0 V_s) [1 + (q/k_D)^2]^{-1} [\epsilon^{(2)}]^2 \quad (8)$$

A subscript PR has been added to designate those fluctuations associated with the photorefractive effect. Equation 8 is the central result of Reference 10. It provides the extension of our previous investigations of light-scattering noise in Kerr media to materials exhibiting the photorefractive effect.

3.4 LIGHT-SCATTERING FLUCTUATIONS IN PHOTOREFRACTIVE MEDIA ASSOCIATED WITH THE OPTICAL KERR EFFECT

Dielectric fluctuations arise in all media (including photorefractives) that exhibit a Kerr-effect (Ref. 4) and, therefore, contribute to light-scattering noise. These fluctuations originate from thermal fluctuations in the density, which through the Clausius-Mossotti constant $\partial\epsilon/\partial\rho$ induce corresponding fluctuations in the dielectric constant independent of the photorefractive effect (Ref. 5). From Reference 5

$$\langle |\delta\epsilon(q)|^2 \rangle_K = 8\pi kT\epsilon_2(q)/V_s = (8\pi kT\epsilon_2/V_s) [1 + (q/q_0)^2]^{-1} \quad (9)$$

where $\epsilon_2(q)$ is the Kerr coefficient and q_0 is the reciprocal correlation length. Generally, for Kerr media $q/q_0 \ll 1$ and this is true for the photorefractive media whose noise properties were studied (Ref. 11). The inequality breaks down when the correlation length approaches the wavelength of light as can occur close to a critical point (the case for which Eq. 9 was originally derived in Ref. 5). The purpose of including the general result here is to note its similarity with Equation 8 for the dielectric fluctuations associated with the photorefractive effect. Apart from the physical distinction between the correlation length and the Debye screening length in the two models, the forms differ only by a nondimensional factor $2\epsilon_0 \epsilon_2 / [\epsilon^{(2)}]^2$.

3.5 ESTIMATES OF DYNAMIC RANGE AND COMPARISON WITH EXPERIMENT

The methods developed in the preceding subsections are illustrated in this subsection for the write and readout of a simple sinusoidal grating using the configuration shown in Figure 3. For the writing beam configuration of Figure 3, the intensity modulation ratio is:

$$m = 2(I_1 I_2)^{1/2} / (I_1 + I_2) \quad (10)$$

where I_1 and I_2 are the intensities for the pump (I_1) and signal (I_2) beams. For light of wave vector $K_1 = K_2 = K$, the resulting grating is of wave vector $q = |q|$:

$$q = 2K \sin(\theta/2) \quad (11)$$

where θ is the angle between the writing beams. Both K and θ are measured in the material with refractive index n_R .

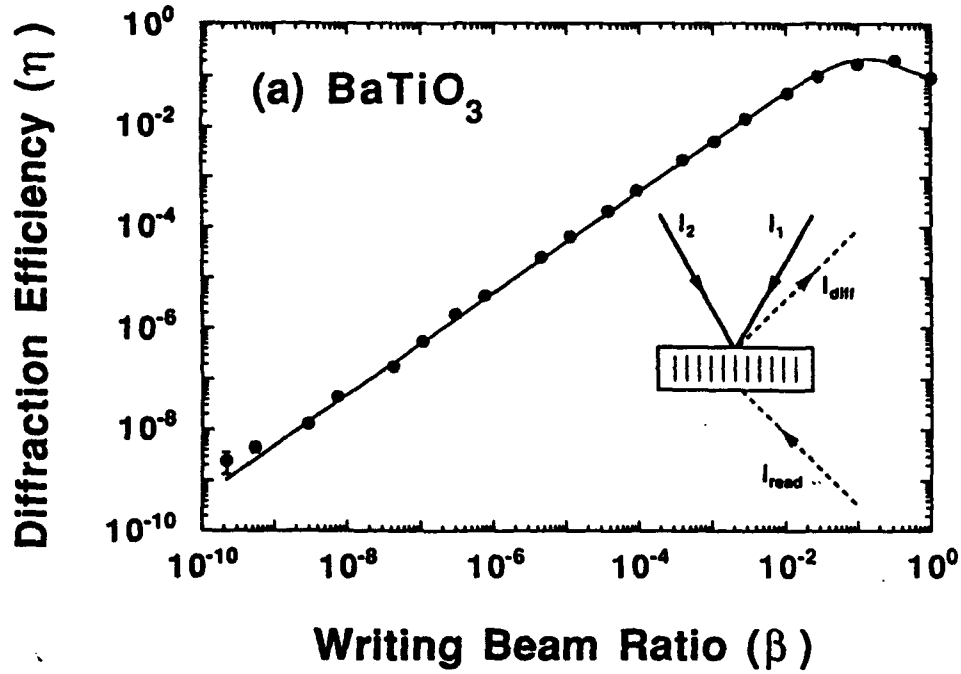


Figure 3. Measurements of dynamic range (from Ref. 11).

In the read stage (Fig. 3), the intensity of the diffracted beam (signal plus noise) is proportional to the square of the total grating amplitude

$$I_{\text{diff}} \sim (a_1 + \delta a_1)^2 \quad (12)$$

where a_1 and δa_1 are the amplitudes of the signal and noise grating components, respectively (Ref. 10):

$$a_1 = -(kTq/e) [1 + (q/k_D)^2]^{-1} \epsilon^{(2)} m \quad (13)$$

The noise grating component is Gaussian distributed with mean

$$\langle \delta a_1 \rangle = 0 \quad (14a)$$

and variance

$$\langle |\delta a_1|^2 \rangle = 2 \langle |\delta \epsilon|^2 \rangle \quad (14b)$$

The factor of 2 in Equation 14b corrects for averaging the square of the sinusoidal spatial dependence of $\delta\epsilon$ over the beam interaction volume. The right-hand side of Equation 14b is evaluated using Equation 8 or 9, depending on whether the noise in question is associated with the Kerr or photorefractive effects.

Experimentally, it is expedient to conduct measurements under the condition that $q = k_D$ since it follows from Equation 13 that the diffraction efficiency is maximized when this condition is satisfied. Under this condition the signal-to-noise ratio (Ref. 10) from is $n_0 V_s m^2 / 4$, which equals unity for a writing beam intensity ratio $I_2/I_1 = 1/(n_0 V_s)$. Figure 4 from Reference 10 shows a calculation of light-scattering noise in the diffracted read beam for BaTiO₃ under the maximum diffraction efficiency condition. The figure shows the logarithm of the diffracted read beam power (in arbitrary units due to the unknown prefactor in Eq. 12) versus the logarithm of the writing beam ratio I_2/I_1 . The beam interaction volume was set equal to the product of the beam cross section area and the interaction length. For the present calculation, the beam diameter was set at 0.15 cm and the interaction length at 0.2 cm, corresponding to the experimental measurement conditions used in Reference 11. Other parameters used in the calculation, which were chosen as representative of BaTiO₃, are listed in Reference 10. As described below, the light-scattering fluctuations associated with the Kerr effect are relatively less important for BaTiO₃ and were omitted from the calculation of Figure 4. This will not always be the case for other photorefractive materials as shown below.

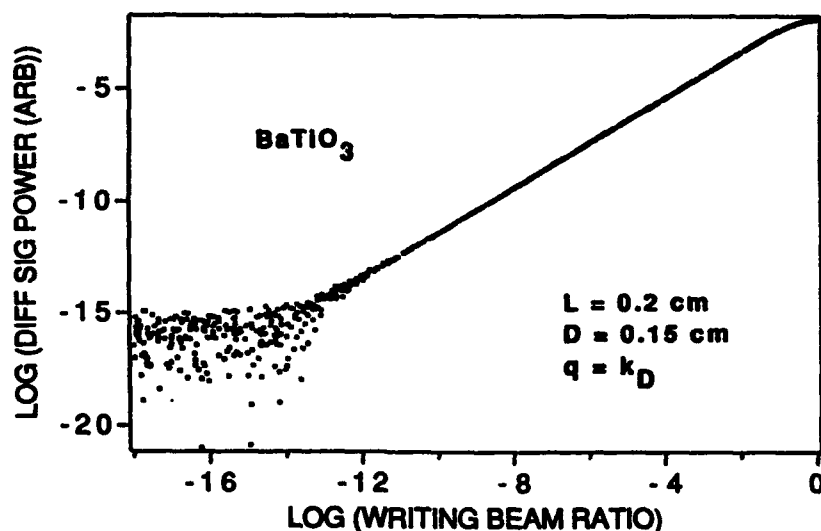


Figure 4. Light-scattering noise simulation (from Ref. 10).

To obtain Figure 4, the right-hand side of Equation 14b for the noise variance was evaluated using Equation 8 with $q = k_D$. To generate the figure, the x-coordinate (log writing beam ratio) was randomly selected, with uniform distribution along the scale of the figure. Next, the signal grating amplitude a_1 was obtained from Equation 13 with m from Equation 10. Finally, a value for δa_1 was sampled from the Gaussian distribution having mean and variance specified by Equations 14a and 14b. Gaussian probability sampling was achieved using a standard computer program incorporating the Box-Muller transformation for the generation of normal deviates from random numbers sampled uniformly on the interval $\{0,1\}$. The above procedure was repeated a thousand times to obtain an equal number of points for good statistical sampling of the noise.

Expansion of the right-hand side of Equation 12 gives three terms, each corresponding to a different region seen in Figure 4. The first term (a_1^2) dominates in the high probe power (low noise) region. In this case, the linear behavior (with unit slope) predicted from Equation 10 for $I_2 < 0.1 I_1$ is observed. As the probe power is reduced further, the next-to-leading term in the expansion ($2a_1\delta a_1$) begins to play a role. This term, which vanishes on time averaging, results in a symmetric distribution of scatter about the average diffracted beam power due to noise. This behavior is seen in the mild noise region of Figure 4. With still further reduction of probe power (i.e., reduction of a_1), the third term in the expansion (δa_1^2) begins to dominate. This last term, which does not vanish on time averaging, results in a diffracted power due entirely to noise. The resulting scatter is independent of the power in the probe since in this region the signal grating amplitude is much smaller than the RMS fluctuation amplitude due to noise. This effect is best seen in the smallest writing beam ratio range of Figure 4. The probe power level for which the signal-to-noise ratio is unity may be computed analytically. For the present values of V_s and n_0 , one obtains $I_2/I_1 = 5.9 \times 10^{-15}$ for $S/N_{PR} = 1$.

Equations 8 and 9 are compared for their relative importance in limiting the dynamic range of a photorefractive medium. Setting $(m_1^2)_K = \alpha(m_1^2)_{PR}$ one obtains for α :

$$\begin{aligned}\alpha &= \{2\epsilon_0 \epsilon_2 / [\epsilon^{(2)}]^2\} [1 + (q/k_D)^2] \\ &= \{4\epsilon_0 n_2 / (n_R^7 r^2)\} [1 + (q/k_D)^2]\end{aligned}\quad (15)$$

For BaTiO_3 , the parameters collected in Reference 10 yield a value of 0.035 for the expression in curly brackets and dynamic range is limited by thermal fluctuations in the space-charge field. For different materials and/or different writing beam configurations, the curly bracketed expression in Equation 15 may easily exceed unity; in which case light-scattering noise associated with the Kerr effect will dominate. Values of α are computed for several other photorefractive materials

in Reference 11. There one finds α values of 0.93 for KNbO_3 , 1.56 for BSKNN, and 3.75 for SBN; all for the maximum diffraction efficiency condition $q/k_D=1$ (Table 1). Thus for KNbO_3 and BSKNN, it is predicted that the thermal light-scattering fluctuations associated with the Kerr and photorefractive effects are of comparable size, while for SBN, fluctuations associated with the Kerr effect are of greater importance to limiting dynamic range.

Table 1. Calculated fundamental limit on the dynamic range due to the various noise sources discussed.

Type of Noise	Minimum Beam Ratio	BaTiO ₃	BSKNN-11	KNbO ₃	SBN:60
Photon Shot Noise	$\beta_{\phi, \min}$	5.3×10^{-18}	3.1×10^{-17}	4.9×10^{-17}	3.4×10^{-17}
Photorefractive Noise	$\beta_{\text{pr}, \min}$	2.6×10^{-15}	2.3×10^{-14}	1.4×10^{-15}	6.4×10^{-16}
Kerr Noise	$\beta_{\text{kerr}, \min}$	3.0×10^{-16}	3.6×10^{-14}	1.3×10^{-15}	2.4×10^{-15}

Finally, note that there will be a photon shot noise contribution arising from fluctuations in the incident intensity of the weak writing beam when the latter becomes sufficiently small that few photons from this beam arrive during the time required for photorefractive grating formation (Ref. 11). The photon shot noise limits to the minimum writing beam ratio were evaluated for each of the various photorefractive materials listed above and were in the 10^{-16} to 10^{-17} range (Ref. 11). Thus, for these materials, the photon shot noise is predicted to be about 1–2 orders of magnitude smaller than the thermal noise associated with either the Kerr or photorefractive effects. The results presented in this section suggest a very large dynamical range for photorefractive materials that should prove useful in optical signal processing applications.

Experimental measurements for the dynamic range using BaTiO₃ as the recording medium are shown in Figure 3 from Reference 11 (note the similarity to the theoretical calculations of Fig. 4). In this case the measured dynamic range is large but not as large as predicted due to the limitations of detector noise in the experiments. The presently available measurements, therefore, serve only as an upper bound to the fundamental noise limits of photorefractive media. Note that the noise properties of photorefractives are qualitatively different from those of Kerr media. For the latter, light-scattering noise is significant at room temperatures even for signal powers in the

milliwatt range. Differences are predominantly in the physical mechanisms underlying formation of the signal grating (Ref. 10). Finally, note that analytic expressions for the signal-to-noise ratio, based on the preceding results, provide the means for predicting the channel capacity of a photorefractive medium (bits/sec) for signal processing applications.

4.0 GENERAL THEORY OF LIGHT-SCATTERING NOISE IN KERR MEDIA

An overview of light-scattering fluctuations and their connection to nonlinear optical response may be gained through an examination of the Maxwell equations governing beam propagation in a nonlinear medium:

$$\nabla \times \mathbf{E}(\mathbf{r},t) = -(1/c)\partial\mathbf{H}(\mathbf{r},t)/\partial t \quad (16a)$$

$$\nabla \times \mathbf{H}(\mathbf{r},t) = (1/c)\partial\mathbf{D}(\mathbf{r},t)/\partial t \quad (16b)$$

with

$$\mathbf{D}(\mathbf{r},t) = [\epsilon_0 + \delta\epsilon(\mathbf{r},t) + \epsilon_2 \overline{\mathbf{E}}^2(\mathbf{r},t)] \mathbf{E}(\mathbf{r},t) \quad (16c)$$

In these equations, $\mathbf{E}(\mathbf{H})$ is the total electric (magnetic) field vector; ϵ_0 (ϵ_2) is the linear (nonlinear) dielectric constant of the medium; $\mathbf{D}(\mathbf{r},t)$ is the displacement vector; and the overbar implies a time average that is long compared to an optical period, but short compared to all other time scales that enter the problem. Equation 16c contains both the nonlinear contribution and the fluctuation contribution to the dielectric constant. The symbols $\delta\epsilon$ and $\Delta\epsilon = \overline{\mathbf{E}}^2$ are used throughout this report to designate variations in the dielectric constant of the medium due to spontaneous fluctuations and to field-induced response, respectively. The fluctuation contribution plays a role in nonlinear optics analogous to the current or voltage fluctuations that give rise to Johnson noise in electrical systems. Both sources of noise are thermal in origin and proportional to kT . In the present case, fluctuations in the linear dielectric constant give rise to noise as they result in the formation of spontaneous gratings that are "read" by the applied laser fields to give a scattered light component that is indistinguishable from the desired output of the nonlinear optical device.

4.1 LIGHT-SCATTERING FLUCTUATIONS AND NONLINEAR OPTICAL RESPONSE

At nonzero temperature T , thermal fluctuations in the linear dielectric constant of the optical Kerr medium give rise to fluctuation gratings capable of scattering incident radiation. More precisely, the fluctuations in the linear dielectric constant, $\delta\epsilon(\mathbf{r},t)$, can be decomposed into grating components, $\delta\epsilon(\mathbf{q},t)$:

$$\delta\epsilon(\mathbf{r},t) = \sum \delta\epsilon(\mathbf{q},t) e^{-i\mathbf{q}\cdot\mathbf{r}} \quad (17)$$

with

$$\delta\epsilon(\mathbf{q}) = (1/V_s) \int e^{i\mathbf{q}\cdot\mathbf{r}} \delta\epsilon(\mathbf{r}) d^3\mathbf{r} \quad (18)$$

where the summation is over all grating wave vectors \mathbf{q} , and the integral is over the beam interaction volume V_s .

For an isotropic Kerr medium with local interactions

$$\epsilon(\mathbf{r}) = \epsilon_0 + \epsilon_2 \bar{E}^2(\mathbf{r}) \quad (19)$$

and Fourier transformation (Eq. 18) gives

$$\epsilon(\mathbf{q}) = \epsilon_0 \delta(\mathbf{q}) + \epsilon_2 E^2(\mathbf{q}) \quad (20)$$

A nonlocal generalization of Equation 19 may be written in terms of the convolution integral:

$$\epsilon(\mathbf{r}) = \epsilon_0 + \int \epsilon_2(\mathbf{r} - \mathbf{r}') E^2(\mathbf{r}') d^3\mathbf{r}' \quad (21)$$

for an isotropic medium. Fourier transformation gives

$$\epsilon(\mathbf{q}) = \epsilon_0 \delta(\mathbf{q}) + \epsilon_2(\mathbf{q}) E^2(\mathbf{q}) \quad (22)$$

This result is identical in form to Equation 20 except for the \mathbf{q} -dependence in ϵ_2 , which becomes important when the range of correlations in the medium approaches the wavelength of light (Ref. 5).

The remainder of this section shows that the fluctuation-dissipation theorem provides a fundamental closure relation between the nonlinear coefficient ϵ_2 and the statistical distribution determining the fluctuations $\delta\epsilon$ for incorporation into Equation 16c.

4.2 APPLICATION OF THE FLUCTUATION-DISSIPATION THEOREM

Preliminary to applying the fluctuation-dissipation theorem, the appropriate conjugate variables must be defined. For this purpose, it is sufficient to note that the energy change in the medium due to the nonlinear polarization is of the form

$$U(\mathbf{r},t) = -(1/8\pi) \Delta\epsilon(\mathbf{r},t) \bar{E}^2(\mathbf{r},t) \quad (23)$$

where $\Delta\epsilon$ is the change in the dielectric constant in the presence of an applied laser field. Accordingly, the field energy variable $u(\mathbf{r},t) = (1/8\pi) \bar{E}^2$ is conjugate to $\Delta\epsilon$ and one may define the complex frequency-dependent susceptibility χ_ϵ such that:

$$\Delta\epsilon(q,\Omega) = \chi_\epsilon(q,\Omega) u(q,\Omega) \quad (24)$$

with $\chi_\epsilon = \chi_\epsilon' + i \chi_\epsilon''$. In particular, it follows from Equation 24 for a Kerr medium ($\Delta\epsilon(q,0) = \epsilon_2(q)E^2(q)$) that $\chi_\epsilon(q,0) = 8\pi \epsilon_2(q) = \chi_\epsilon'(q,0)$.

The power, P, expended by the applied fields on the medium electric polarization is proportional to the imaginary component of the susceptibility

$$P = \langle \mathbf{E} \cdot d\mathbf{P}_{NL}/dt \rangle = V_s \Omega \chi_\epsilon'' u^2/2 \quad (25)$$

where \mathbf{P}_{NL} is the nonlinear polarization and the angular brackets denote averaging over the beam interaction volume V_s . The fluctuation-dissipation theorem is (Ref. 6)

$$\chi_\epsilon''(q,\Omega) = (1/2\hbar) [1 - \exp(-\hbar\Omega/kT)] S_\epsilon(q,\Omega) \quad (26a)$$

which in the classical limit ($kT \gg \hbar\Omega$), reduces to the form

$$\chi_\epsilon''(q,\Omega) = (\Omega/2kT) S_\epsilon(q,\Omega) \quad (26b)$$

where

$$S_\epsilon(q,\Omega) = V_s \int \langle \delta\epsilon(q,0) \delta\epsilon(q,t) \rangle e^{-i\Omega t} dt \quad (27)$$

is the spectral density of the fluctuations in the linear dielectric constant $\delta\epsilon$ that give rise to light scattering noise.

Each of the preceding results may readily be expressed in tensor component form for applications to anisotropic media. The scalar u , for example, is then replaced by the Maxwell stress tensor in its most general form, with $\Delta\epsilon$ and χ_ϵ represented by second and fourth ranked tensors, respectively.

Equations 25 through 27 are the appropriate generalization of our previously derived static susceptibility relation, which was limited to degenerate beam interactions and did not include power dissipation. To recover the special case, first note that the real and imaginary components of χ_ϵ satisfy the Kramers-Kronig relation (Ref. 6):

$$\begin{aligned} \chi_\epsilon'(q,0) &= (1/\pi) \int \chi_\epsilon''(q,\Omega) / \Omega d\Omega \\ &= (kT)^{-1} V_s \langle |\delta\epsilon(q)|^2 \rangle \end{aligned} \quad (28)$$

where the last equality follows upon substitution from Equations 26b and 27 for the imaginary susceptibility component and the integral is over both positive and negative frequencies. From Equation 28, and the above assignment of $\chi_e(q,0)$ for a Kerr medium,

$$\chi_e'(q,0) = 8\pi \epsilon_2(q) \quad (29)$$

the static susceptibility relation (Ref. 4)

$$\langle |\delta\epsilon(q)|^2 \rangle = 8\pi kT \epsilon_2(q) / V_s \quad (30)$$

is immediately obtained. Equation 30 is the closure relation required for incorporation into Equation 16c. Its present derivation is both more direct and more general than the thermodynamic fluctuation approach used in Reference 5, which also allows for possible q -dependence in the Kerr coefficient due to nonlocal interaction.

For the case of photorefractive media described in the preceding subsection, dielectric fluctuations arise from thermal fluctuations in the space-charge field through the electro-optic effect (Ref. 10). In this case, fluctuation variance is given by an expression which differs from the right-hand side of Equation 30 only by the nondimensional factor $[\epsilon^{(2)}]^2 / 2\epsilon_0 \epsilon_2(0)$ where $\epsilon^{(2)}$ is the Pockels coefficient and the q dependence takes the same form as that obtained previously for the nonlocal interaction described in Reference 5, with the range of correlations set by the Debye screening length.

5.0 APPLICATIONS TO TWO-WAVE MIXING AND COMPARISON WITH EXPERIMENT

The first measurements of noise during two-wave mixing in a Kerr medium are reported in References 8 and 9. Experiments were conducted at visible wavelengths using an aqueous suspension of shaped microparticles as the nonlinear medium. Theoretical calculations and computer simulations using a stochastic model for light-scattering noise gave excellent agreement with the experimental results. This section presents a summary of those results.

5.1 THEORY

A schematic illustration of the two-wave mixing geometry for amplification of a weak signal is shown in Figure 5. Two laser beams of frequencies ω_1 and $\omega_2 = \omega_1 - \Omega$ propagate through the nonlinear medium and create a moving density grating response that preferentially deflects energy from the high-frequency to the low-frequency beam. The solid lines depict the crests of the field-induced grating of wave vector $q = K_1 - K_2$. Dashed lines represent a spontaneous moving grating arising from thermal fluctuations in the medium. Some of these thermal gratings will be in a proper configuration to deflect energy from the high-frequency to the low-frequency wave, in a manner that is indistinguishable from the signal, to give a noise component represented by the dashed arrow in the figure. For two incident plane waves, the total field is of the form

$$\begin{aligned} E(r,t) = & e_1 E_1(r) \cos[K_1 \cdot r - \omega_1 t + \theta_1(r)] \\ & + e_2 E_2(r) \cos[K_2 \cdot r - \omega_2 t + \theta_2(r)], \end{aligned} \quad (31)$$

where e_j , $E_j(r)$, and $\theta_j(r)$ are the unit polarization vector, slowly varying amplitude, and slowly varying phase of wave j .

The signal and noise gratings depicted schematically in Figure 5 are quantitatively described as follows: For the signal grating (Ref. 8)

$$\Delta \epsilon(r,t) = a_1 \cos(q \cdot r - \Omega t) + b_1 \sin(q \cdot r - \Omega t) \quad (32)$$

where

$$a_1 = (e_1 \cdot e_2) \epsilon_2 E_1 E_2 / [1 + (\Omega \tau)^2] \quad (33)$$

and

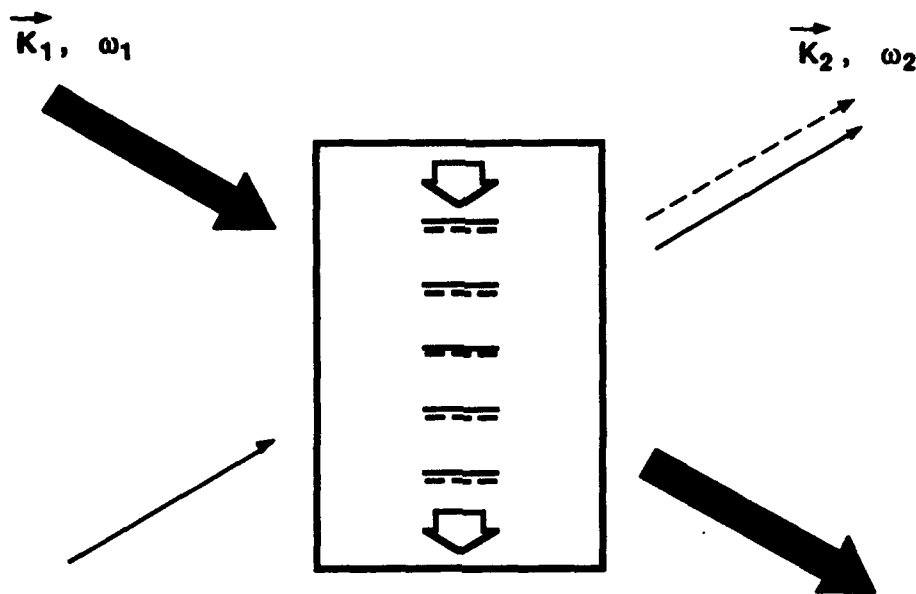


Figure 5. Two-wave mixing geometry.

$$b_1 = -(\mathbf{e}_1 \cdot \mathbf{e}_2) \epsilon_2 E_1 E_2 \Omega \tau / [1 + (\Omega \tau)^2] \quad (34)$$

are the in-phase and $\pi/2$ out-of-phase grating coefficients, respectively, for a Debye relaxation medium. For the noise grating, the coefficients a_Ω and b_Ω are statistically distributed according to the bottom set of equations in Table 2 (Ref. 8).

The preceding expressions may be combined to obtain the total variation in dielectric constant from both signal and noise contributions. When the result is substituted into the wave equation, the various terms in the displacement vector give rise to scattering of electromagnetic energy into different modes, characterized by specific wave vectors and frequencies. The most significant contribution results from those terms that have minimum phase mismatch. Denoting these by $D(\mathbf{r}, t)$, one finds (Ref. 8)

$$\begin{aligned} D(\mathbf{r}, t) = & \epsilon_0 \mathbf{E}(\mathbf{r}, t) + (1/2) (a_1 + a_\Omega) E_1(\mathbf{r}) \cos(\mathbf{K}_2 \cdot \mathbf{r} - \omega_2 t + \theta_2) \mathbf{e}_1 \\ & + (1/2) (a_1 + a_\Omega) E_2(\mathbf{r}) \cos(\mathbf{K}_1 \cdot \mathbf{r} - \omega_1 t + \theta_1) \mathbf{e}_2 \\ & - (1/2) (b_1 + b_\Omega) E_1(\mathbf{r}) \sin(\mathbf{K}_2 \cdot \mathbf{r} - \omega_2 t + \theta_2) \mathbf{e}_1 \\ & + (1/2) (b_1 + b_\Omega) E_2(\mathbf{r}) \sin(\mathbf{K}_1 \cdot \mathbf{r} - \omega_1 t + \theta_1) \mathbf{e}_2. \end{aligned} \quad (35)$$

Table 2. Signal and noise gratings for two-wave mixing.

$$\mathbf{q} = \mathbf{K}_1 - \mathbf{K}_2 \quad \Omega = \omega_1 - \omega_2$$

Signal grating (field induced)

$$\Delta\epsilon(\mathbf{q}, \Omega) = a_1 \cos(\mathbf{q} \cdot \mathbf{r} - \Omega t) + b_1 \sin(\mathbf{q} \cdot \mathbf{r} - \Omega t)$$

$$a_1 = \epsilon_2 (\mathbf{e}_1 \cdot \mathbf{e}_2) E_1 E_2 / [1 + (\Omega\tau)^2]$$

$$b_1 = -\epsilon_2 (\mathbf{e}_1 \cdot \mathbf{e}_2) E_1 E_2 \Omega\tau / [1 + (\Omega\tau)^2]$$

Noise grating (thermal)

$$a_\Omega \cos(\mathbf{q} \cdot \mathbf{r} - \Omega t) + b_\Omega \sin(\mathbf{q} \cdot \mathbf{r} - \Omega t)$$

$$\langle a_\Omega \rangle = \langle b_\Omega \rangle = 0$$

$$\begin{aligned} \langle a_\Omega^2 \rangle &= \langle b_\Omega^2 \rangle = (\tau/\pi) \langle |\delta\epsilon(\mathbf{q})|^2 \rangle / [1 + (\Omega\tau)^2] \\ &= (8kT\epsilon_2/V_s) / [1 + (\Omega\tau)^2] \end{aligned}$$

Equation 35 describes an instantaneous polarization, or snapshot of the medium, that includes contributions from both signal and phase-matched noise gratings. According to the adiabatic approximation, this polarization will remain sensibly constant over time periods that are short in comparison with the medium response time, $\tau = \Gamma^{-1}$, but still long compared with the transit time of light through the medium.

Inserting Equation 35 into the wave equation (Eq. 16), making the slowly varying amplitude and phase approximation, and equating the in-phase and out-of-phase terms, one finds

$$(\mathbf{K}_1 \cdot \nabla) E_1 = K^2/4 \epsilon_0 (b_1 + b_\Omega) (\mathbf{e}_1 \cdot \mathbf{e}_2) E_2 - (\alpha_0/2) E_1 \quad (36a)$$

$$(\mathbf{K}_1 \cdot \nabla) \theta_1 = K^2/4 \epsilon_0 (a_1 + a_\Omega) (\mathbf{e}_1 \cdot \mathbf{e}_2) E_2/E_1 \quad (36b)$$

for the pump wave and

$$(\mathbf{K}_2 \cdot \nabla) E_2 = -K^2/4 \epsilon_0 (b_1 + b_\Omega) (\mathbf{e}_1 \cdot \mathbf{e}_2) E_1 - (\alpha_0/2) E_2 \quad (36c)$$

$$(K_2 \cdot \nabla) \theta_2 = K^2/4 \epsilon_0 (a_1 + a_\Omega) (e_1 \cdot e_2) E_1/E_2 \quad (36d)$$

for the signal. These equations are identical to those obtained previously except for the presence of the new noise terms, which result in fluctuations in both amplitude and phase. In the case that the pump is much stronger than the signal ($E_1 \gg E_2$), these fluctuations are much more important for the signal than for the pump beam. The last terms in Equations 36a and 36c include the effect of nonsaturable background loss, where α_0 is the attenuation coefficient for loss of light intensity. For a nonabsorbing, isotropic medium in which losses are due to scattering alone,

$$\alpha_0 = (\omega^4/6\pi c^4) V_s \langle |\delta\epsilon(q)|^2 \rangle = 4/3 (2\pi v/c)^4 kT \epsilon_2 \quad (37)$$

where v is the optical frequency.

Finally, one may obtain an expression for the power dissipated in the medium during two-wave mixing. For a uniformly moving grating, the stored energy in the medium is constant and the dissipated power per unit volume is (Ref. 8)

$$P = \langle E \cdot dP/dt \rangle = -(1/16\pi) b_1 (e_1 \cdot e_2) E_1 E_2 \Omega. \quad (38)$$

Equation 38 predicts an asymptotic level of power dissipation for $\Omega\tau$ approaching infinity. This follows from the functional form of b_1 , exhibited in Equation 34, which in turn is a consequence of the Debye relaxation model. As expected, the fluctuating noise gratings make no contribution to power dissipation.

5.2 EXPERIMENTAL RESULTS

Measurements of gain and noise were made using liquid suspensions of polytetrafluoroethylene (PTFE) shaped microparticles as artificial Kerr media. Light-induced, particle-orientation rearrangements account for optically-induced birefringence with consequent large nonlinear optical response. Several studies have been carried out to characterize the linear and nonlinear optical properties of these suspensions, and good agreement between theoretical predictions and experimental results was found. This agreement is due in large part to the characteristics of the suspensions, which fit an independent particle-single orientational relaxation time Debye model remarkably well. Particles are ellipsoidal in shape (the dimensions are $0.4 \times 0.2 \times 0.2 \mu\text{m}$) and the particle polarizability tensor has corresponding symmetry. The particle suspensions are highly monodisperse, and interparticle interactions are negligible even at relatively high volume fractions (0.1–2%). In the present experiments, a 1 percent volume fraction of PTFE particles suspended in a 65/35 water/glycerol host-liquid mixture was typically used. This mixture was

chosen because it matches the average value of the particle refractive index $n_0 = 1.376$, thus minimizing the importance of light-scattering fluctuations due to the isotropic part of the particle polarizability.

Figure 6 shows the experimental setup for nondegenerate two-wave mixing. The pump and the probe waves are provided by splitting the 514-nm TEM₀₀ output of a cw Argon-ion laser into a 1-W power pump beam and a 50-mW probe beam. The two beams eventually intersect at the focus of the lens (L) within the sample at an angle of 5 deg. The beam waist size is about 100 μm and the interaction length is 0.1 cm. Before entering the sample, the polarization direction of the pump beam is rotated perpendicular to that of the probe so that only the orientational particle gratings are generated in the suspension by the beam interference pattern.

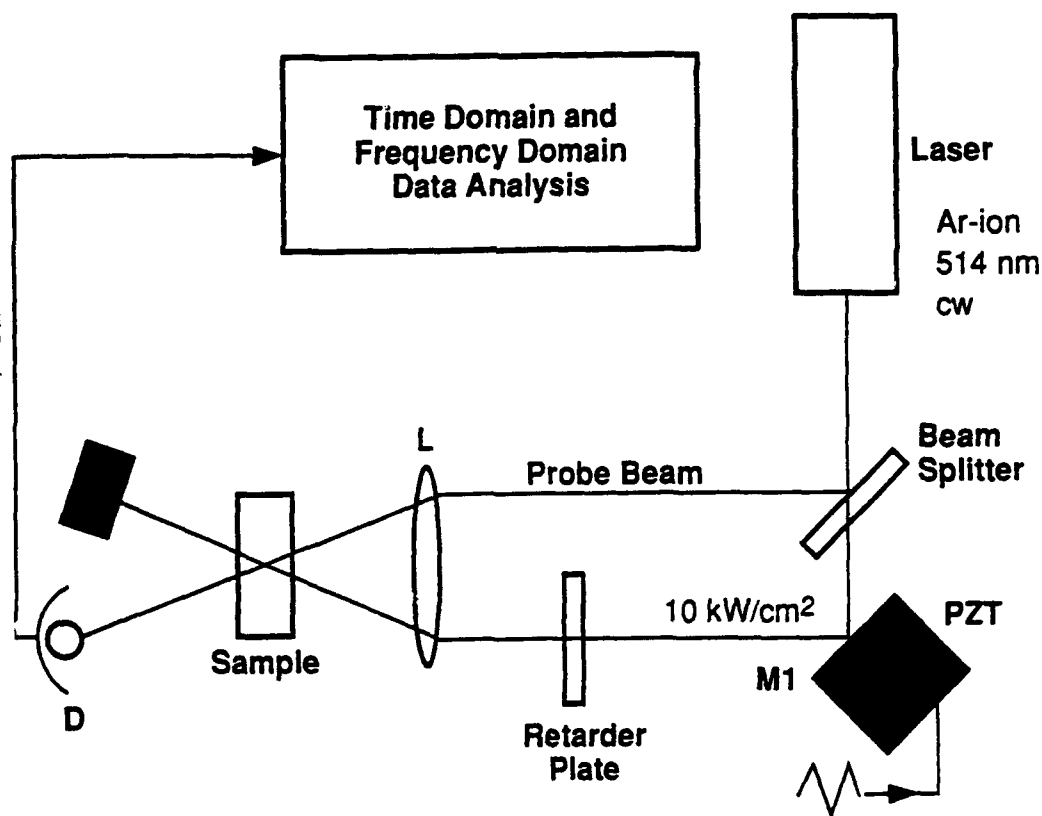


Figure 6. Schematic diagram of the two-wave mixing optical arrangement and electronics for noise analysis. (L: focusing lens; M1: 100% mirror; PZT: piezoelectric transducer; D: photodiode.)

The angular frequency shift Ω required for the nondegenerate beam configuration is provided to the pump beam by the mirror M1 that is mounted to a piezoelectric transducer (PZT). A triangular 8-Hz high-voltage wave is fed through the PZT to produce a periodic linear displacement of the mirror with constant, sign-inverting speed. The consequent square-wave-like angular frequency shift can be varied by either changing the amplitude or the frequency of the mirror displacement. The periodic intensity gain of the probe beam is revealed by a low-noise photodiode (D). A polarizer is placed before the photodiode to remove the polarized component of the pump light scattered into the probe beam by the isotropic particle fluctuations. After a low-pass electrical amplification (-3 dB at 3 kHz), the photodiode output is fed both into a digital oscilloscope and into a 12-bit, PC-interfaced spectrum analyzer. For each value of the frequency shift, the average value of the intensity gain was obtained by a digital average on the oscilloscope while the spectral properties of the gain fluctuations were monitored on the spectrum analyzer. Implementing this setup, particular care had to be taken to damp mechanical vibrations that could add random phase shifts to the beams thus introducing spurious noise in the gain process.

Figure 7 (top) shows the experimental results for the probe intensity gain and noise fluctuations. Pump light intensity in the sample was approximately 10 kW/cm^2 while the transmitted probe power in the absence of the pump beam was 50 mW. The vertical bars report the transmitted probe-beam power in watts as a function of the nondimensional frequency shift $\Omega\tau$, where $\tau = \tau_R = 8.9 \text{ ms}$ is the orientational response time as determined through independent measurements. Each vertical bar is centered on the average value of the transmitted power and the bar length reports the root-mean-square (RMS) value of the noise fluctuations on the same scale. The RMS noise fluctuations are also shown in the figure on an expanded scale for clarity (full circles) and were obtained by integration of the noise power spectrum over a collection bandwidth of 60 Hz. The smooth curve is a fit to the data using $\sigma(P_2) = C [1 + (\Omega\tau)^2]^{-1/2}$, which is the form expected from the theory and will now be described.

For two incident plane waves, the total field is of the form given by Equation 31. Insertion into the wave equation, making the slowly varying amplitude and phase approximation, and equating the in-phase and out-of-phase terms, gives a set of four coupled equations (Eq. 36) describing the evolution of the two amplitudes and two phases, which may be integrated using the stochastic noise model (Ref. 6). In the absence of pump depletion and background loss, an analytic solution to these equations may be obtained, which is sufficient for comparison with the present measurements. Here, the solution is required for the weak probe beam $E_2(L)$, where L is the beam interaction length, in the presence of a nondepleted pump E_1 . The result, from Reference 8, is

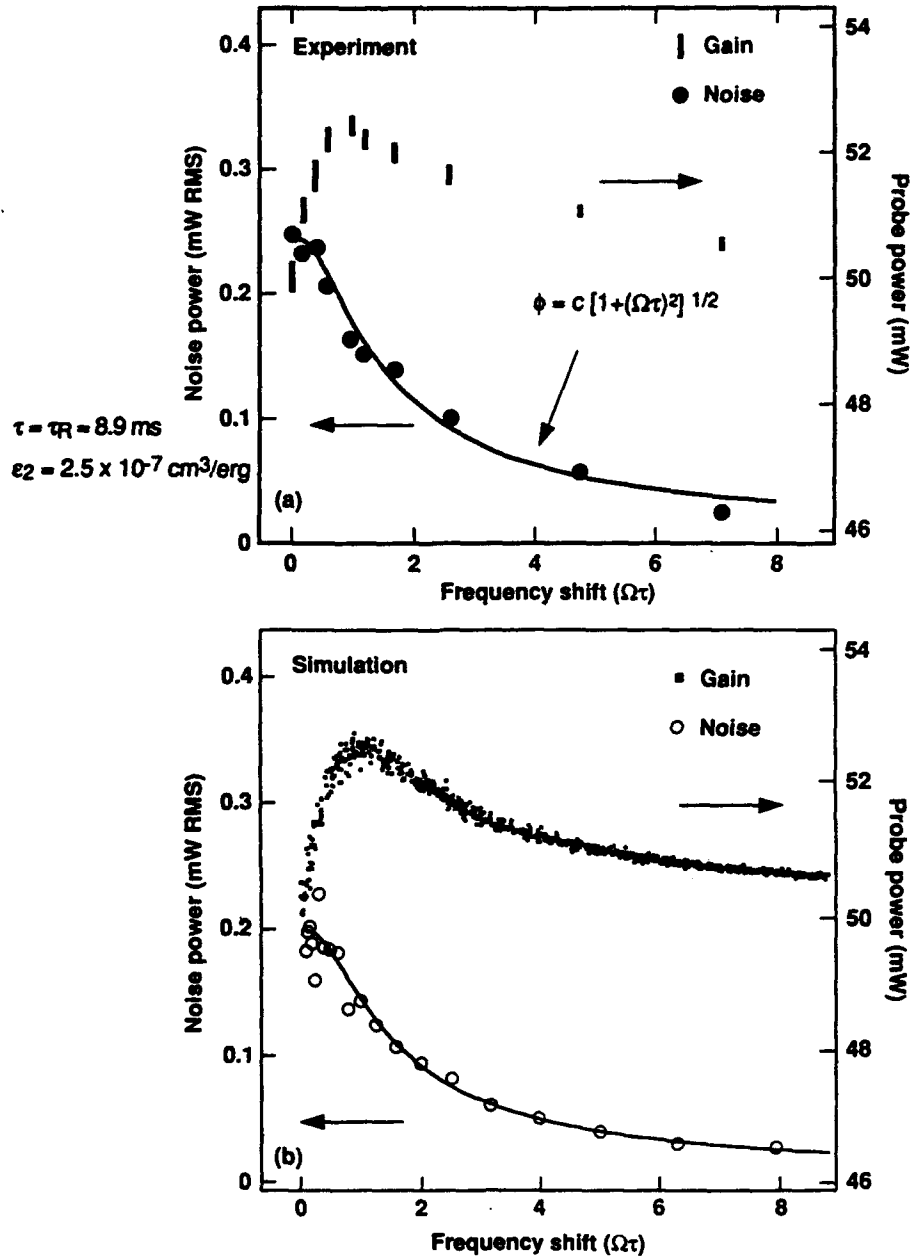


Figure 7. Comparison of experimental and simulation results for two-wave mixing gain and light-scattering noise.

$$E_2(L) = \exp(\alpha_S L) E_2(0) + (\alpha_N / \alpha_S) [\exp(\alpha_S L) - 1] E_1 \quad (39)$$

where

$$\alpha_S = (K/4\epsilon_0) \epsilon_2 E_1^2 \Omega \tau / [1 + (\Omega \tau)^2] = h \Omega \tau / [1 + (\Omega \tau)^2] \quad (40)$$

and

$$\alpha_N = (K/4\epsilon_0) b_\Omega \quad (41)$$

In Equation 40, $K = |K_1| = |K_2|$, ϵ_0 is the background dielectric constant, ϵ_2 is the Kerr coefficient, and $\Omega = \omega_1 - \omega_2$. The last equality in Equation 41 defines h . In Equation 41, b_Ω is the quadrature component for a thermal fluctuation grating having the same orientational configuration as the signal grating, thereby giving rise to a scattered light component that is indistinguishable from the signal beam. Note that ϵ_2 and b_Ω are off-diagonal components of second-rank tensors, but may be treated here as scalars since in each case only one tensor component is selected by the fixed polarizations of the writing beams.

Inspection of Equations 39-41 reveals that fluctuations in b_Ω cause fluctuations in the amplitude of the transmitted probe. In addition to b_Ω , there is an in-phase noise component a_Ω , which results in fluctuations in the phase. The mean and variances for the grating amplitude fluctuations (Table 2) are derived in Reference 8:

$$\langle a_\Omega \rangle = \langle b_\Omega \rangle = 0 \quad (42a)$$

$$\langle a_\Omega^2 \rangle = \langle b_\Omega^2 \rangle = (2\tau B) \langle |\delta\epsilon(q)|^2 \rangle / [1 + (\Omega\tau)^2] \quad (42b)$$

where the dependence on frequency difference Ω and response time τ follows our assumption of a single relaxation time Debye medium. The right-hand side of Equation 42b gives the noise power over a frequency bandwidth B and is obtained by multiplying the result of Reference 8, which gives the noise power on a per unit angular frequency basis, by $2\pi B$. The right-hand side of Equation 42b may be evaluated in terms of the nonlinear dielectric constant, or Kerr coefficient, ϵ_2 using Equation 30, where $q = K_1 - K_2$ is the wave vector of the matched thermal fluctuation grating and V_s is the scattering or beam interaction volume determined from the product of the beam cross section area A and the interaction length L .

For comparison with experiment, Equation 39 was evaluated numerically using the stochastic noise model (Ref. 6). The one adjustable parameter in the theory is the Kerr coefficient, and this is obtained here from a fit to the gain curve, not to the noise. The gain curve shown in Figure 7 (bottom) was obtained using $\epsilon_2 = 3.6 \times 10^{-7} \text{ cm}^3/\text{erg}$, in reasonable agreement with the estimate for this quantity obtained from previous nonlinear optics measurements: $\epsilon_2 = 2.5 \times 10^{-7} \text{ cm}^3/\text{erg}$. The remaining conditions used in the calculations are the same as those described above for the experiment. The simulation proceeds by the following steps: (1) A value for $\Omega\tau$ is selected and Equation 42 is used to obtain the mean and variance for the noise amplitude fluctuations over the

measurement bandwidth $B = 60$ Hz. The fluctuations are assumed to be Gaussian and sampling is achieved using a standard computer algorithm incorporating the Box-Muller transformation for the generation of normal deviates from random numbers sampled uniformly on the interval $(0,1)$. (2) Equation 39 is evaluated for each sampled b_Ω to give a solution for $E_2(L)$ and corresponding amplified signal power $P_2(L)$. Steps 1 and 2 are repeated on the order of a thousand times to obtain a good statistical sampling of the noise over the full $\Omega\tau$ range of interest. Results of the calculation are shown in Figure 7 (bottom). Note that both the experimental and theoretical gain profiles follow frequency dispersion curves characteristic of the Debye relaxation model. More importantly, there is excellent agreement between theory and experiment in regard to the RMS values of the noise fluctuations, including their dependence on frequency shift. This agreement is remarkable, in view of the lack of adjustable parameters in the theory.

Squaring the right-hand side of Equation 39 gives noise terms proportional to α_N and to α_N^2 . In most cases of interest, $E_2(0)$ is sufficiently large that the latter term may be neglected, leaving the cross term containing the product $E_1 E_2(0)$. Then one finds for the standard deviation of the power fluctuations in the amplified signal in the limit of small gain:

$$\sigma(P_2) = (4\pi\tau B)^{1/2} (hL)^{1/2} [kT \nu P_2(0)]^{1/2} [1 + (\Omega\tau)^2]^{-1/2} (hL \ll 1) \quad (43)$$

Since the maximum power gain ($G = e^{hL}$) in the experiment is 1.05, the small gain approximation used to derive Equation 7 is valid for the present discussion. Equation 43 shows the origin of the $[1 + (\Omega\tau)^2]^{-1/2}$ dependence seen in the measurements and provides an explicit form for the prefactor C . Here $P_2(0)$ is the incident signal power, P_2 is the fluctuating signal power at $z = L$, and $\sigma(P_2)$ is the standard deviation of P_2 : $\sigma(P_2) = [\langle P_2^2 \rangle - \langle P_2 \rangle^2]^{1/2}$.

The solid curve in Figure 7 (bottom) displays the analytical result given by Equation 43. The open circles are numerical results obtained by Gaussian sampling using the stochastic noise model—each circle represents an RMS value computed for 100 samples at a fixed value of $\Omega\tau$. The simulated noise is in excellent agreement with both the analytical and experimental results. Finally, note that the noise fluctuations decrease monotonically with frequency unlike the average gain, which peaks at $\Omega\tau = 1$.

Equation 43 implies that the RMS amplitude of the noise fluctuations increases with the square root of the incident probe power $P_2(0)$. Figure 8 reports the experimental values of the RMS noise power (triangles) as a function of the probe power for $\Omega\tau = 0$. As can be seen, the square-root dependence (full line) is well verified over a decade range.

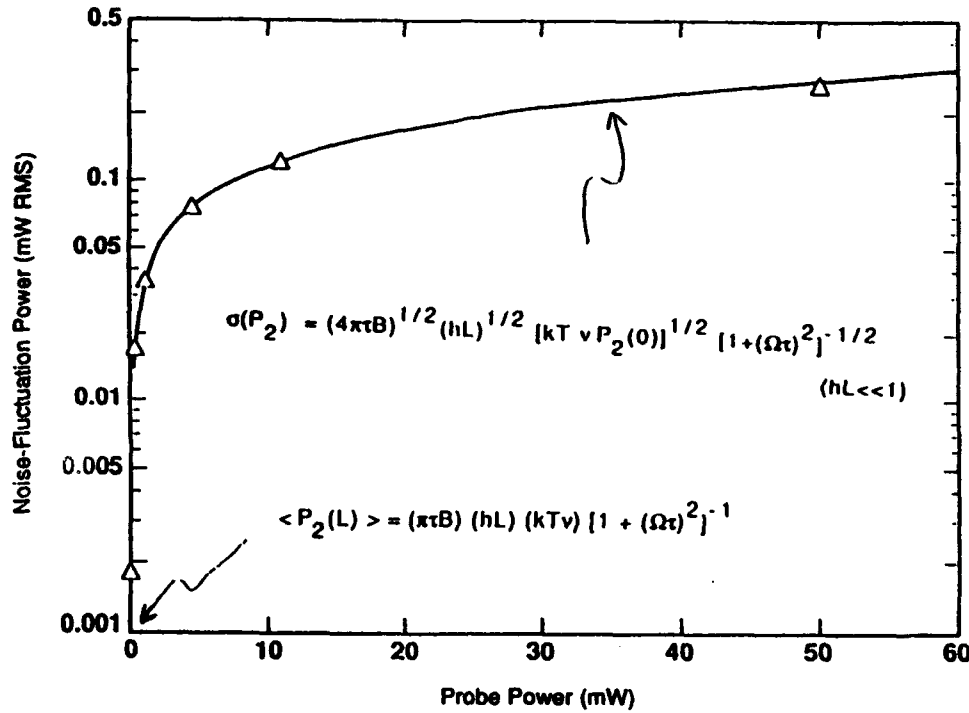


Figure 8. The RMS noise power as a function of probe power for $\Omega t = 0$. (The experimental data points [triangles] follow a square-root dependence on the probe power [solid curve]. The single data point on the ordinate gives the RMS noise power measured in the absence of the probe beam.)

Theory predicts that the RMS probe-power fluctuations should satisfy Equation 43 as long as light-induced gratings are dominant with respect to thermal gratings. Equation 39 shows that for an incident probe power of zero, output fluctuations will occur proportional to α_N^2 . Note that the noise fluctuations proportional to α_N^2 , unlike those proportional to α_N , do not vanish on time averaging. Analysis similar to that used to derive Equation 43 gives

$$\langle P_2(L) \rangle = (\pi \tau B) (hL) (kTv) [1 + (\Omega \tau)^2]^{-1} \quad (44)$$

where $\langle P_2(L) \rangle$ is the average power of the noise at $z = L$. The factor (kTv) is the Nyquist expression for the thermal noise power radiated by a channel having a bandwidth equal to the optical frequency ν . Equation 44 yields a predicted average noise power at zero probe power of $0.2 \mu\text{W}$ due entirely to scattered pump light. The stochastic noise model sampling confirms this result and gives an RMS power of $0.28 \mu\text{W}$. The RMS noise power was measured at zero signal power by blocking the probe. The result of this measurement ($1.8 \mu\text{W RMS}$) is represented by the single data point appearing on the ordinate of Figure 8. At this low noise level, the discrepancy between theory and experiment is much greater than for the previous comparisons made with the probe beam on and most likely is due to extraneous sources of noise being present in the measurement.

In summary, the first measurements of light-scattering noise during two-wave mixing in a Kerr medium were described. Excellent quantitative agreement between the experimental results and theoretical predictions was obtained, with no adjustable parameters, using the stochastic noise model for thermal light-scattering noise (Ref. 6) and its extension to two-wave mixing (Ref. 8).

6.0 RESEARCH DIRECTIONS

Table 3 and Figures 9-11 describe the recently completed results obtained for resonant media. The model used is that of the damped harmonic oscillator. Noise arises from both thermal and quantum fluctuations of the oscillator polarizability that give rise to scattered light. Our previous results for general Kerr media are recovered as a special case in the high damping limit. For example, the response curves shown in Figure 11 are identical to Equations 33 and 34 for the Debye relaxation model Kerr medium.

Table 3. Light-scattering noise in resonant media.

- Requires a unified description of quantum-thermal noise

Quantum correction

$$S_{\epsilon}(q, \Omega) = V_s \int \langle \delta\epsilon(q, 0) \delta\epsilon(q, t) \rangle e^{-i\Omega t} dt$$

$$S_{\epsilon}(q, -\Omega) = V_s \int \langle \delta\epsilon(q, t) \delta\epsilon(q, 0) \rangle e^{-i\Omega t} dt$$

$$\text{since } \langle \delta\epsilon(q, t) \delta\epsilon(q, 0) \rangle = \langle \delta\epsilon(q, 0) \delta\epsilon(q, t) \rangle^* .$$

Condition of detailed balance:

$$S_{\epsilon}(q, -\Omega) = \exp(-\hbar\Omega/kT) S_{\epsilon}(q, \Omega)$$

Classically, the correlation function is real and

$$S_{\epsilon}(q, -\Omega) = S_{\epsilon}(q, \Omega).$$

Table 3 shows the fundamental nature of the changes that need to be made in the fluctuation theorem to include quantum effects. The results described thus far in this report apply to the thermal noise limit ($\Omega \ll kT/\hbar$) typical of slow media having large nonlinear optical coefficients. In this limit, the maximum frequency difference Ω is limited by the medium response time and quantum noise effects, which can be dominant for Raman amplifiers (Ref. 11), may be neglected

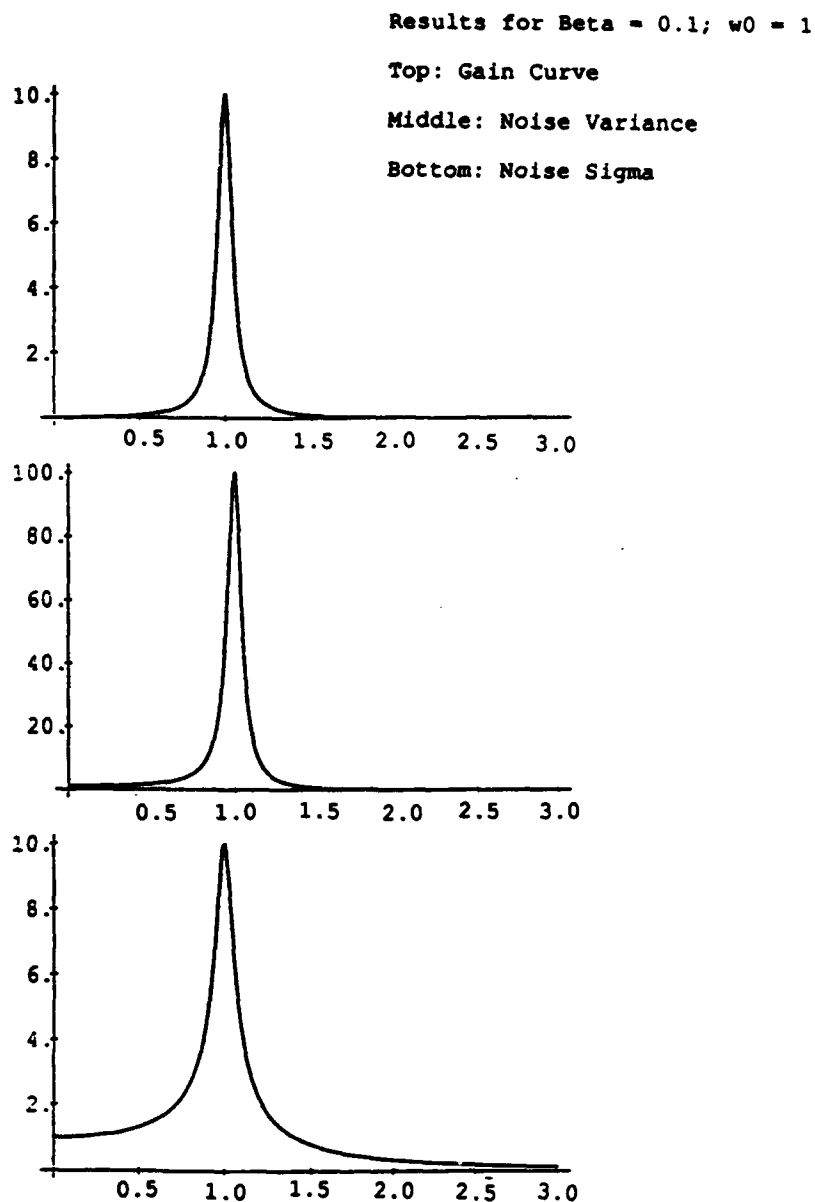


Figure 9. Results for damped oscillator, low damping.

as these are orders of magnitude smaller than the noise described here. A soon-to-be-completed publication will extend the theory to cases for which Ω is comparable to or greater than kT/\hbar in a unified treatment of quantum-thermal noise.

With further development, the results may serve as the scientific basis necessary for the design of new low-noise nonlinear optical materials—probably with best prospects in the general classes of photorefractive polymers and charge transfer media. Furthermore, the results can provide the foundation for investigations into the noise properties of optical communication channels and

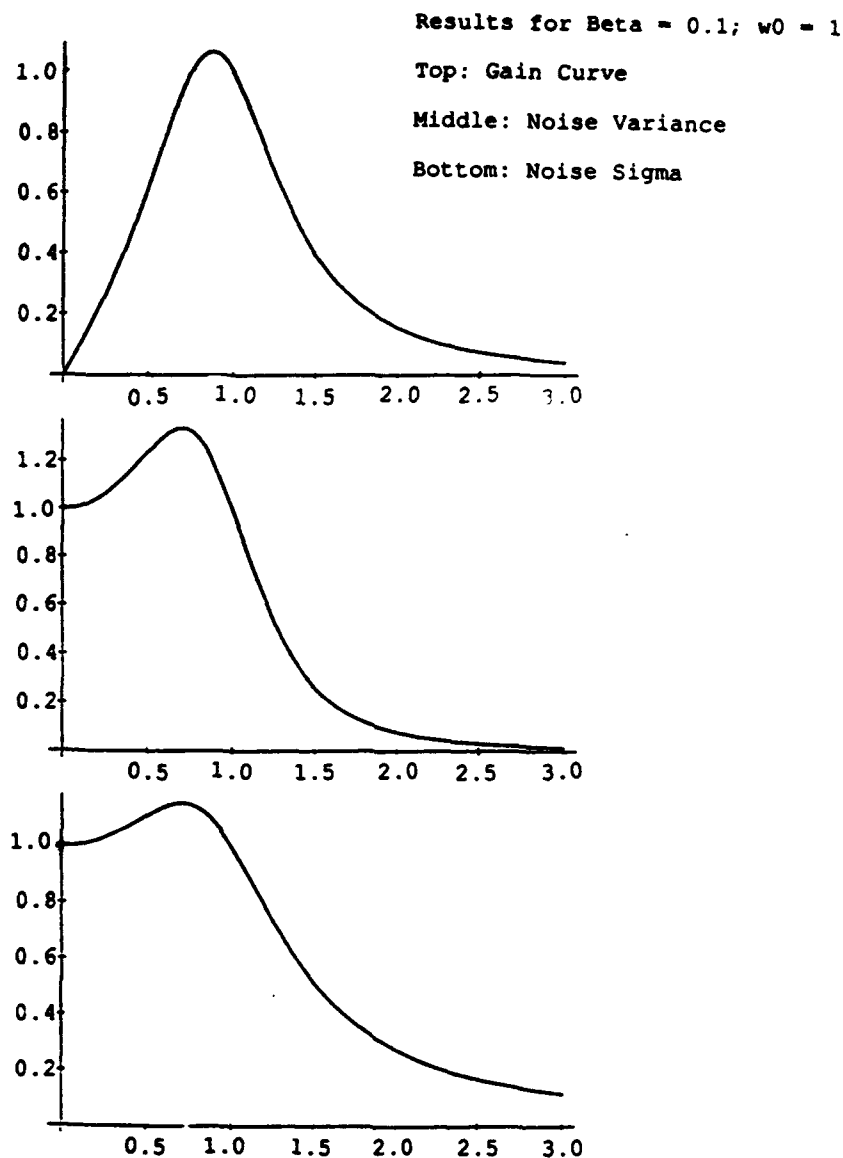


Figure 10. Results for damped oscillator, intermediate damping.

optical storage media. These investigations can include determination of the Shannon channel capacity (some work along these lines has already been carried out for photorefractive media) and new applications of optical signal processing and computing (e.g., the optical wavelet transform and optical methods for signal and image compression).

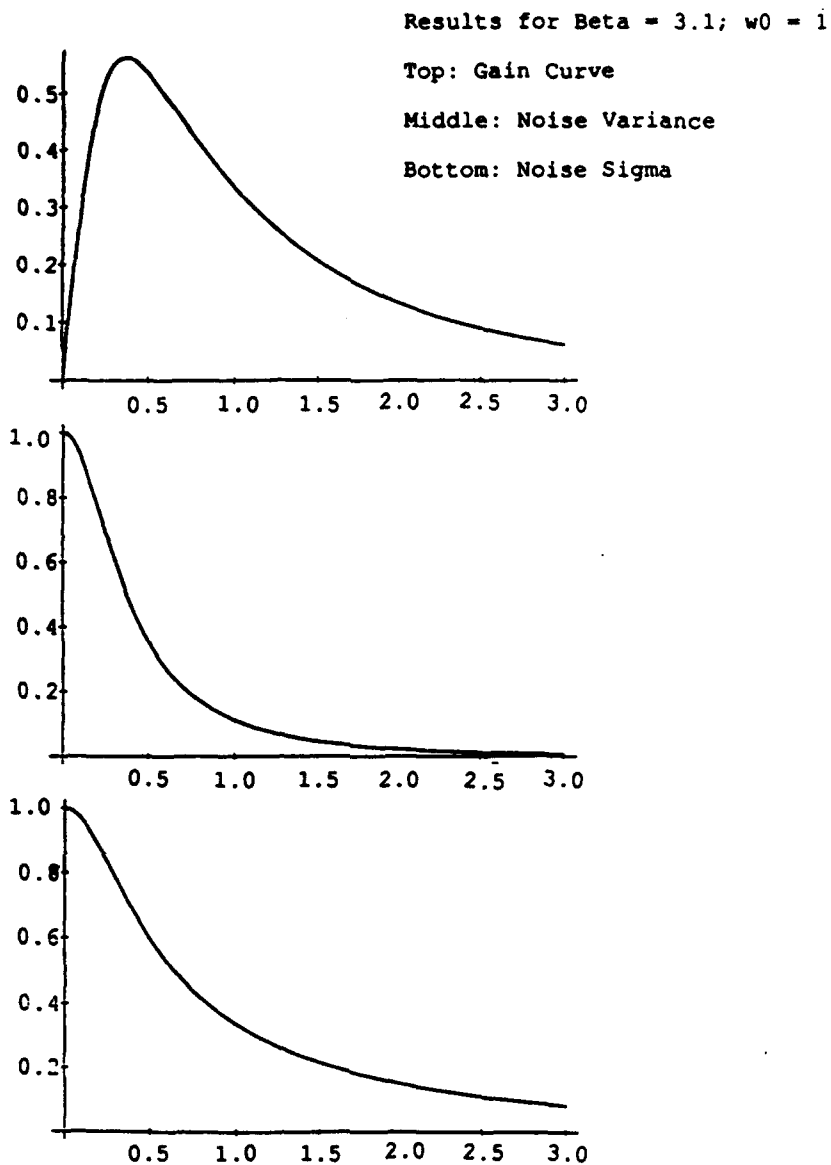


Figure 11. Results for damped oscillator, high damping.

REFERENCES

1. Sternklar, S., Glick, Y., and Jackel, S., "Noise limitations of Brillouin two beam coupling: theory and experiment," J. Opt. Soc. Am., B9, 391 (1992).
2. McGraw, R. and Rogovin, D., "Light-Scattering Fluctuations and Noise in an Artificial Kerr Medium," SPIE, 739, 100-104 (1987).
3. McGraw, R. and Rogovin, D., "Four-Wave Mixing and Thermal Noise," *Proc. 3rd Int. Laser Science Conference, Atlantic City, NJ*; in *Optical Science and Engineering Series 9*, R. G. Lerner, ed., 253-255 (1987).
4. McGraw, R., Rogovin, D., and Gavrielides, A., "Light-scattering limitations for phase conjugation in optical Kerr media," Appl. Phys. Lett., 54, 199 (1989).
5. McGraw, R., "Light scattering and nonlinear optical response near a critical point," Phys. Rev., A42, 2235-2247 (1990).
6. McGraw, R., "Stochastic models for light-scattering noise in nonlinear optical Kerr media," Phys. Rev., A45, 3250-3259 (1992).
7. Rogovin, D., McGraw, R., and Gavrielides, A., "Role of thermal light scattering fluctuations in nondegenerate two-wave mixing," Appl. Phys. Lett., 55, 1937 (1989).
8. McGraw, R., "Light-scattering noise limits to two-wave mixing gain in Kerr media," J. Opt. Soc. Am., B9, 98-103 (1992).
9. Pizzoferrato, R., McGraw, R., and Rogovin, D., "Measurements of light-scattering noise accompanying two-wave mixing in a Kerr medium," Phys. Rev., A47, R2476-R2479 (1993).
10. McGraw, R., "Light-scattering fluctuations and thermal noise in photorefractive media," Phys. Rev., A46, 1810-1820 (1992).
11. Chang, T. Y., Hong, J. H., Vachss, F., and McGraw, R., "Dynamic range of photorefractive gratings," J. Opt. Soc. Am., B9, 1744-1751 (1992).

12. Kukhtarev, N.V., Markov, V.B., Odulov, S.G., Soskin, M.S., and Vinetskii, V.L., "Holographic storage in electrooptic crystals. 1. steady state," Ferroelectrics, **22**, 949 (1979).
13. Feinberg, J., Heiman, D., Tanguay, A. R., Jr., and Hellwarth, R. W., "Photorefractive effects and light-induced charge migration in barium titanate," J. Appl. Phys., **51**, 1297 (1980).